Composites: Part B 70 (2015) 99–112

Contents lists available at ScienceDirect

Composites: Part B

journal homepage: www.elsevier.com/locate/compositesb

Stochastic free vibration analyses of composite shallow doubly curved shells – A Kriging model approach

Sudip Dey *, Tanmoy Mukhopadhyay, Sondipon Adhikari

College of Engineering, Swansea University, Swansea SA2 8PP, United Kingdom

ARTICLE INFO

Article history:
Received 26 July 2014
Received in revised form 9 October 2014
Accepted 27 October 2014
Available online 1 November 2014

Keywords:
A. Polymer–matrix composites (PMCs)
B. Vibration
C. Finite element analysis (FEA)
C. Computational modelling
Uncertainty quantification

ABSTRACT

This paper presents the Kriging model approach for stochastic free vibration analysis of composite shallow doubly curved shells. The finite element formulation is carried out considering rotary inertia and transverse shear deformation based on Mindlin's theory. The stochastic natural frequencies are expressed in terms of Kriging surrogate models. The influence of random variation of different input parameters on the output natural frequencies is addressed. The sampling size and computational cost is reduced by employing the present method compared to direct Monte Carlo simulation. The convergence studies and error analysis are carried out to ensure the accuracy of present approach. The stochastic mode shapes and frequency response function are also depicted for a typical laminate configuration. Statistical analysis is presented to illustrate the results using Kriging model and its performance.

1. Introduction

Composite materials are extensively employed in aerospace, marine, automotive, construction and many other industries due to its high specific stiffness and strength along with weight sensitivity and cost-effectiveness. Laminated composite materials are generally fabricated from unidirectional plies of given shape, geometry and material properties. Due to the inherent complexity, laminated composite shell is difficult to manufacture accurately according to its exact design specifications, resulting in undesirable uncertainties which in turn affect the vibration characteristics of components. It involves many sources of uncertainty associated with material properties variation and boundary conditions variability. In general, the fibre and matrix are fabricated with three basic steps namely tape, layup and curing. The properties of constituent material vary statistically due to lack of precision and accuracy to maintain the exact properties in each layer of the laminate. The misalignment of ply-orientation, intra-laminate voids, incomplete curing of resin, excess resin between plies, excess matrix voids and porosity resulting from machine, human and process inaccuracy are the common mode of uncertainties incurred during manufacturing process. Moreover the defects caused due to such variability can compromise the performance of composite components, which in turn lead to the use of more conservative designs that do not fully exploit the performance and environmental opportunities offered by composites. As a result, the free vibration responses of such laminated composite shells show the fluctuation from its mean value. In general, additional factor of safety is considered by the designer to account for such unpredictable frequency responses which may lead to result in either an unsafe or an ultraconservative design. Thus the structural stability is subjected to considerable element of risk. Such risk is involved as the variability in the estimated output (say natural frequency) resulting from the uncertainties in the values of random input material properties and fibre parameters in each layer of laminated composites. Uncertainties from a single input parameter may propagate and influence to another input parameters and the final system output may have a significant cascading effect due to accumulation of risk. This variability can result in significant deviations from the expected output. Therefore, it is essential to estimate the variability in natural frequencies together with the expected performance characteristic value (say mean deterministic natural frequency) to ensure the operational safety. Even though assessment of natural frequency of composite structures has gained wide spectrum of attention and applications, the treatment of uncertainties to quantify and analyse the same for composite shallow doubly curved shells has received little attention. Hence the present study is aimed to quantify the variability in first three natural frequencies of laminated composite shallow doubly curved shells using Kriging model approach.

The general broad categories of uncertainties are aleatoric (due to variability in the system parameters), epistemic (due to lack of knowledge of the system) and prejudicial (due to absence of variability characterization), respectively. In general, Monte Carlo

* Corresponding author.
E-mail addresses: infosudip@gmail.com, S.Dey@swansea.ac.uk (S. Dey).

http://dx.doi.org/10.1016/j.compositesb.2014.10.043
1359-8368/

simulation (MCS) technique is employed to generate the output parameter (say natural frequency) considering large sample size. Although the uncertainty in material and geometric properties can be computed by the original MCS method, it is inefficient and incurs high computational cost. To mitigate this lacuna, present analysis employed the Kriging technique to map the uncertainties efficiently. Its purpose is to estimate response quantities (say natural frequency) based on randomness considered in input parameters (ply orientation angle, elastic modulus, mass density, shear modulus and Poisson's ratio). The present approach is based on constructing surrogate model. Those surrogate models represent an estimate for the relation between the input parameters of the finite element model and response quantities of interest. The pioneering specific model and related algorithm is developed by using mathematical and statistical methods to obtain Kriging [1–3] solutions. Of late, the basis of design and analysis of experiments are also investigated [4,5]. Kriging model is found to be employed in geostatistics and optimization [2,6–9]. A Kriging based approach is studied for locating a sampling site in the assessment of air quality [10] while the correct Kriging variance is estimated by bootstrapping [11]. Further studies also extended for estimating recoverable reserves by ordinary multi-gaussian Kriging [12] and as probabilistic models in design [13]. Later on, the uncertainty quantification of dynamic adaptive sampling is studied based on Kriging surrogate models [14]. From the open literature, it is found that the Kriging criterion provides a rational means for creating experimental designs for surrogate modelling. Such modelling for uncertainty quantification in natural frequency of laminated composites using Kriging approach has not yet encountered. However, the dynamic stability of uncertain laminated beams subjected to subtangential loads is studied by Goyal and Kapania [15] and subsequently numerous studies are carried out on free vibration of laminated composites [16–20]. Fang and Springer [21] studied on the design of composite laminates by a Monte Carlo method and several investigations are made on doubly curved shells [22–24]. Talha and Singh [25] investigated on buckling statistics of functionally graded plates with uncertain material properties in thermal environments while Hu and Peng [26] studied on maximization of fundamental frequency of axially compressed laminated curved panels with cutouts. The probabilistic approach is employed for design of composite wings including uncertainties [27] and a stochastic model is developed to predict the strength and crack path of composites [28]. The comprehensive review on reliability of composites [29], the probabilistic progressive failure model [30] and the static and dynamic analyses of laminated doubly-curved and degenerate shells and panel [31] are also investigated. In contrast, the probabilistic approaches for representation of interval uncertainty [32] and boundary discontinuous Fourier solution for plates and doubly curved panels using a higher order theory [33] are studied while stochastic analysis of composites is also investigated [34,35]. The response surface methods are employed addressing the parameters uncertainty for composite [36] and fuzzy parametric uncertainty [37] while the effect of ply level material uncertainty is investigated on composite elastic couplings in laminated plates [38].

To the best of the authors' knowledge, there is no literature available which deals with composite structural dynamics using Kriging model for uncertainty quantification of shallow doubly curved shells. To fill up this apparent void, the present analyses employed the finite-element approach to study the stochastic free vibration characteristics of graphite–epoxy composite cantilever shallow doubly curved shells by using Kriging surrogate model. In present analysis, selective representative samples are drawn using Latin hypercube sampling algorithm over the entire domain ensuring good prediction capability of the constructed surrogate model. The Kriging algorithm is developed to quantify uncertainties in natural frequencies of cantilever composite shallow doubly curved shells and its efficacy is compared with direct Monte Carlo simulation (MCS) technique. An eight noded isoparametric quadratic element with five degrees of freedom at each node is considered in finite element formulation. The number of sample runs required to generate the stochastic free vibration responses is catastrophically reduced by using the present approach.

2. Governing equations

In present study, a composite cantilever shallow doubly curved shells with uniform thickness '*t*' and principal radii of curvature R_x and R_y along *x*- and *y*-direction respectively is considered as furnished in Fig. 1. Based on the first-order shear deformation theory, the displacement field of the shells may be described as

$$\begin{aligned} u(x,y,z) &= u^0(x,y) - z\theta_x(x,y) \\ v(x,y,z) &= v^0(x,y) - z\theta_y(x,y) \\ w(x,y,z) &= w^0(x,y) = w(x,y) \end{aligned} \tag{1}$$

where $\mathbf{u}^0$, $\mathbf{v}^0$, and $\mathbf{w}^0$ are displacements of the reference plane and $\boldsymbol{\theta}_\mathbf{x}$ and $\boldsymbol{\theta}_\mathbf{y}$ are rotations of the cross section relative to **x** and **y** axes, respectively. Each of the thin fibre of laminae can be oriented at an arbitrary angle '**θ**' with reference to the **x**-axis. The constitutive equations [39] for the shell are given by

$$\{F\} = [D(\bar{\omega})]\{\varepsilon\} \tag{2}$$

where force resultant $\{F\} = \{N_x, N_y, N_{xy}, M_x, M_y, M_{xy}, Q_x, Q_y\}^T$

$$\{F\} = \left[\int_{-h/2}^{h/2} \{\sigma_x, \sigma_y, \tau_{xy}, \sigma_{xz}, \sigma_{yz}, \tau_{xyz}, \tau_{xz}, \tau_{yz}\}\, dz\right]^T$$

and strain $\{\varepsilon\} = \{\varepsilon_x, \varepsilon_y, \varepsilon_{xy}, k_x, k_y, k_{xy}, \gamma_{xz}, \gamma_{yz}\}^T$

$$\text{where } [D(\bar{\omega})] = \begin{bmatrix} A_{11} & A_{12} & A_{16} & B_{11} & B_{12} & B_{16} & 0 & 0 \\ A_{12} & A_{22} & A_{26} & B_{12} & B_{22} & B_{26} & 0 & 0 \\ A_{16} & A_{26} & A_{66} & B_{16} & B_{26} & B_{66} & 0 & 0 \\ B_{11} & B_{12} & B_{16} & D_{11} & D_{12} & D_{16} & 0 & 0 \\ B_{12} & B_{22} & B_{26} & D_{12} & D_{22} & D_{26} & 0 & 0 \\ B_{16} & B_{26} & B_{66} & D_{16} & D_{26} & D_{66} & 0 & 0 \\ 0 & 0 & 0 & 0 & 0 & 0 & S_{44} & S_{45} \\ 0 & 0 & 0 & 0 & 0 & 0 & S_{45} & S_{55} \end{bmatrix} \tag{3}$$

The elements of elastic stiffness matrix $[D(\bar{\omega})]$ can be expressed as

$$\begin{aligned} [A_{ij}(\bar{\omega}), B_{ij}(\bar{\omega}), D_{ij}(\bar{\omega})] &= \sum_{k=1}^{n} \int_{z_{k-1}}^{z_k} [\{\overline{Q}_{ij}(\bar{\omega})\}_{on}]_k [1, z, z^2]\, dz \\ & \quad i,j = 1,2,6 \\ [S_{ij}(\bar{\omega})] &= \sum_{k=1}^{n} \int_{z_{k-1}}^{z_k} \alpha_s [\overline{Q}_{ij}]_k dz \quad i,j = 4,5 \end{aligned} \tag{4}$$

where $\bar{\omega}$ indicates the stochastic representation and α_s is the shear correction factor (=5/6) and $[\overline{Q}_{ij}]$ are elements of the off-axis elastic constant matrix which is given by

$$\begin{aligned} [\overline{Q}_{ij}]_{off} &= [T_1(\bar{\omega})]^{-1} [\overline{Q}_{ij}]_{on} [T_1(\bar{\omega})]^{-T} \quad \text{for } i,j = 1,2,6 \\ [\overline{Q}_{ij}]_{off} &= [T_2(\bar{\omega})]^{-1} [\overline{Q}_{ij}]_{on} [T_2(\bar{\omega})]^{-T} \quad \text{for } i,j = 4,5 \end{aligned} \tag{5}$$

$$[T_1(\bar{\omega})] = \begin{bmatrix} m^2 & n^2 & 2mn \\ n^2 & m^2 & -2mn \\ -mn & mn & m^2 - n^2 \end{bmatrix} \text{ and } [T_2(\bar{\omega})] = \begin{bmatrix} m & -n \\ n & m \end{bmatrix} \tag{6}$$

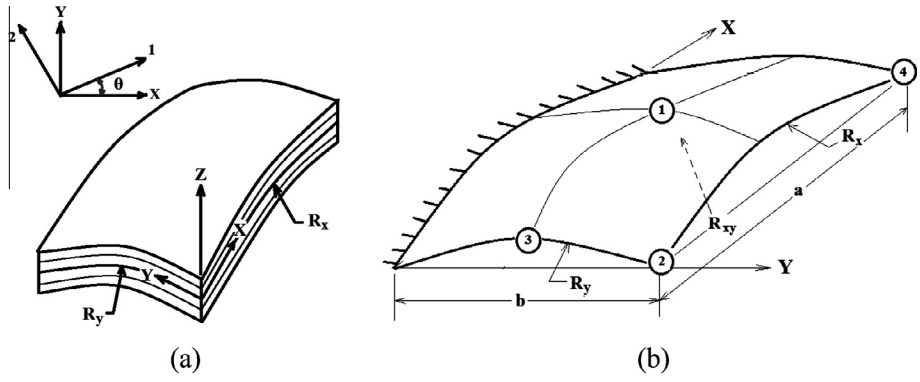

Fig. 1. Laminated composite shallow doubly curved shell model.

in which $m = \mathrm{Sin}\theta(\bar{\omega})$ and $n = \mathrm{Cos}\theta(\bar{\omega})$, wherein $\theta(\bar{\omega})$ is random fibre orientation angle.

$$[Q_{ij}(\bar{\omega})]_{on} = \begin{bmatrix} Q_{11} & Q_{12} & 0 \\ Q_{12} & Q_{12} & 0 \\ 0 & 0 & Q_{66} \end{bmatrix} \text{ for } i,j = 1,2,6$$
$$[\overline{Q}_{ij}(\bar{\omega})]_{on} = \begin{bmatrix} Q_{44} & Q_{45} \\ Q_{45} & Q_{55} \end{bmatrix} \text{ for } i,j = 4,5 \tag{7}$$

where

$$Q_{11} = \frac{E_1}{1 - v_{12}v_{21}} \quad Q_{22} = \frac{E_2}{1 - v_{12}v_{21}} \quad \text{and} \quad Q_{12} = \frac{v_{12}E_2}{1 - v_{12}v_{21}}$$

$$Q_{66} = G_{12} \quad Q_{44} = G_{23} \quad \text{and} \quad Q_{55} = G_{13}$$

The strain–displacement relations for shallow doubly curved shells can be expressed as

$$\begin{Bmatrix} \varepsilon_x \\ \varepsilon_y \\ \gamma_{xy} \\ \gamma_{xz} \\ \gamma_{yz} \end{Bmatrix} = \begin{Bmatrix} \frac{\partial u}{\partial x} - \frac{w}{R_x} \\ \frac{\partial v}{\partial y} - \frac{w}{R_y} \\ \frac{\partial u}{\partial y} + \frac{\partial v}{\partial x} - \frac{2w}{R_{xy}} \\ \theta_x + \frac{\partial w}{\partial x} \\ \theta_y + \frac{\partial w}{\partial y} \end{Bmatrix}, \begin{Bmatrix} k_x \\ k_y \\ k_{xy} \\ k_{xz} \\ k_{yz} \end{Bmatrix} = \begin{Bmatrix} \frac{\partial \theta_x}{\partial x} \\ \frac{\partial \theta_y}{\partial y} \\ \frac{\partial \theta_x}{\partial y} + \frac{\partial \theta_y}{\partial x} \\ 0 \\ 0 \end{Bmatrix} \tag{8}$$

and $\{\varepsilon\} = [B]\{\delta_e\}$

$$\{\delta_e\} = \{u_1, v_1, w_1, \theta_{x1}, \theta_{y1}, \ldots u_8, v_8, w_8, \theta_{x8}, \theta_{y8}\}^T$$

$$\text{where } [B] = \sum_{i=1}^{8} \begin{bmatrix} N_{i,x} & 0 & -\frac{N_i}{R_x} & 0 & 0 \\ 0 & N_{i,y} & -\frac{N_i}{R_y} & 0 & 0 \\ N_{i,y} & N_{i,x} & -\frac{2N_i}{R_{xy}} & 0 & 0 \\ 0 & 0 & 0 & N_{i,x} & 0 \\ 0 & 0 & 0 & 0 & N_{i,y} \\ 0 & 0 & 0 & N_{i,y} & N_{i,x} \\ 0 & 0 & N_{i,x} & N_i & 0 \\ 0 & 0 & N_{i,y} & 0 & N_i \end{bmatrix}$$

where R_{xy} is the radius of curvature in xy-plane of shallow doubly curved shells and k_x, k_y, k_{xy}, k_{xz}, k_{yz} are curvatures of the shell and u, v, w are the displacements of the mid-plane along x, y and z axes, respectively. In case of doubly curved shallow shell elements are employed to model the middle-surface geometry more accurately. An eight noded isoparametric quadratic element with five degrees of freedom at each node (three translations and two rotations) is considered wherein the shape functions ($\mathbf{N_i}$) are as follows [40]

$$\mathrm{N_i} = (1 + \chi\chi_\mathrm{i})(1 + \varsigma\varsigma_\mathrm{i})(\chi\chi_\mathrm{i} + \varsigma\varsigma_\mathrm{i} - 1)/4 \quad (\text{for i} = 1,2,3,4) \tag{9}$$

$$\mathrm{N_i} = (1 - \chi^2)(1 + \varsigma\varsigma_\mathrm{i})/2 \quad (\text{for i} = 5,7) \tag{10}$$

$$\mathrm{N_i} = (1 - \varsigma^2)(1 + \chi\chi_\mathrm{i})/2 \quad (\text{for i} = 6,8) \tag{11}$$

where ς and χ are the local natural coordinates of the element. The mass per unit area for doubly curved shell is expressed as

$$P(\bar{\omega}) = \sum_{k=1}^{n} \int_{z_{k-1}}^{z_k} \rho(\bar{\omega}) dz \tag{12}$$

Mass matrix is expressed as

$$[M(\bar{\omega})] = \int_{Vol} [N][P(\bar{\omega})][N] d(vol) \tag{13}$$

The stiffness matrix is given by

$$[K(\bar{\omega})] = \int_{-1}^{1} \int_{-1}^{1} [B(\bar{\omega})]^T [D(\bar{\omega})][B(\bar{\omega})] d\varsigma d\chi \tag{14}$$

The Hamilton's principle [41] is employed to study the dynamic nature of the composite structure. The principle used for the Lagrangian which is defined as

$$L_f = T - U - W \tag{15}$$

where T, U and W are total kinetic energy, total strain energy and total potential of the applied load, respectively. The Hamilton's principle applicable to non-conservative system is expressed as,

$$\delta H = \int_{p_i}^{p_f} [\delta T - \delta U - \delta W] dp = 0 \tag{16}$$

Hamilton's principle applied to dynamic analysis of elastic bodies states that among all admissible displacements which satisfy the specific boundary conditions, the actual solution makes the functional $\int(T + V)dp$ stationary, where T and W are the kinetic energy and the work done by conservative and non-conservative forces, respectively. For free vibration analysis (i.e., $\delta W = 0$), the stationary value is actually a minimum. In case of a dynamic problem without damping the conservative forces are the elastic forces developed within a deformed body and the non-conservative forces are the external force functions. The energy functional for Hamilton's principle is the Lagrangian (L_f) which includes kinetic energy (T) in addition to potential strain energy (U) of an elastic body. The expression for kinetic energy of an element is expressed as

$$T = \frac{1}{2}\{\dot{\delta}_e\}^T [M_e(\bar{\omega})]\{\dot{\delta}_e\} \tag{17}$$

The potential strain energy for an element of a plate can be expressed as,

$$U = U_1 + U_2 = \frac{1}{2}\{\delta_e\}^T [K_e(\bar{\omega})]\{\delta_e\} + \frac{1}{2}\{\delta_e\}^T [K_{\sigma e}(\bar{\omega})]\{\delta_e\} \tag{18}$$

The Langrange's equation of motion is given by

$$\frac{d}{dt}\left[\frac{\partial L_f}{\partial \delta_e}\right] - \left[\frac{\partial L_f}{\partial \delta_e}\right] = \{F_e\} \tag{19}$$

where $\{F_e\}$ is the applied external element force vector of an element and L_f is the Lagrangian function. Substituting $L_f = T - U$, and the corresponding expressions for T and U in Lagrange's equation, the dynamic equilibrium equation for each element expressed as [42]

$$[M(\bar{\omega})]\{\ddot{\delta}_e\} + ([K_e(\bar{\omega})]) + [K_{\sigma e}(\bar{\omega})]\{\delta_e\} = \{F_e\} \tag{20}$$

After assembling all the element matrices and the force vectors with respect to the common global coordinates, the equation of motion of a free vibration system with n degrees of freedom can expressed as

$$[M(\bar{\omega})][\ddot{\delta}] + [K(\bar{\omega})]\{\delta\} = \{F_L\} \tag{21}$$

In the above equation, $M(\bar{\omega}) \in R^{n\times n}$ is the mass matrix, $[K(\bar{\omega})]$ is the stiffness matrix wherein $[K(\bar{\omega})] = [K_e(\bar{\omega})] + [K_{\sigma e}(\bar{\omega})]$ in which $K_e(\bar{\omega}) \in R^{n\times n}$ is the elastic stiffness matrix, $K_{\sigma e}(\bar{\omega}) \in R^{n\times n}$ is the geometric stiffness matrix (depends on initial stress distribution) while $\{\boldsymbol{\delta}\} \in R^n$ is the vector of generalized coordinates and $\{F_L\} \in R^n$ is the force vector. The governing equations are derived based on Mindlin's theory incorporating rotary inertia, transverse shear deformation. For free vibration, the random natural frequencies $[\omega_n(\bar{\omega})]$ are determined from the standard eigenvalue problem [40] which is represented below and is solved by the QR iteration algorithm,

$$[A(\bar{\omega})]\{\delta\} = \lambda(\bar{\omega})\{\delta\} \tag{22}$$

where

$$[A(\bar{\omega})] = ([K_e(\bar{\omega})] + [K_{\sigma e}(\bar{\omega})])^{-1}[M(\bar{\omega})]$$

$$\lambda(\bar{\omega}) = \frac{1}{\{\omega_n(\bar{\omega})\}^2} \tag{23}$$

It can be also shown that the eigenvalues and eigenvectors satisfy the orthogonality relationship that is

$$\mathrm{x}_l^T[M(\bar{\omega})]\mathrm{x}_j = \lambda_{lj} \quad \text{and} \quad \mathrm{x}_l^T[K(\bar{\omega})]\mathrm{x}_j = \omega_j^2\lambda_{lj} \quad \text{where } l,j = 1,2\ldots n \tag{24}$$

Note that the Kroneker delta functions is given by $\lambda_{lj} = 1$ for $l = j$ and $\lambda_{lj} = 0$ otherwise. The property of the eigenvectors in (24) is also known as the mass orthonormality relationship. The solution of undamped eigenvalue problem is now standard in many finite element packages. This orthogonality property of the undamped modes is very powerful as it allows to transform a set of coupled differential equations to a set of independent equations. For convenience, the matrices are expressed as

$$\begin{aligned} &\Omega(\bar{\omega}) = \mathrm{diag}[\omega_1, \omega_2, \omega_3 \ldots \omega_n] \quad \in \quad R^{n\times n} \\ &\text{and } \mathrm{X}(\bar{\omega}) = [\mathrm{x}_1, \mathrm{x}_2 \ldots \mathrm{x}_n] \quad \in \quad R^{n\times n} \end{aligned} \tag{25}$$

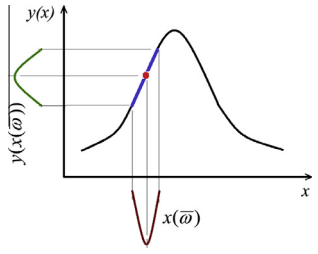

Fig. 2. Simulation model.

where the eigenvalues are arranged such that $\omega_1 < \omega_2$, $\omega_2 < \omega_3$, … $\omega_k < \omega_{k+1}$. The matrix $\mathbf{X}$ is known as the undamped modal matrix. Using these matrix notations, the orthogonality relationships (24) can be rewritten as

$$\mathrm{x}_l^T[M(\bar{\omega})]\mathrm{x}_j = \lambda_{lj} \quad \text{and} \quad \mathrm{x}_l^T[K(\bar{\omega})]\mathrm{x}_j = \omega_j^2\lambda_{lj} \quad \text{where } l,j = 1,2\ldots n \tag{26}$$

$$\mathrm{X}^T[M(\bar{\omega})]\mathrm{X} = \mathrm{I} \quad \text{and} \quad \mathrm{X}^T[K(\bar{\omega})]\mathrm{X} = \Omega^2 \tag{27}$$

where $\mathbf{I}$ is a $(n \times n)$ identity matrix. We use the following coordinate transformation (as the modal transformation)

$$\delta(\bar{\omega})(t) = \mathrm{X}\mathrm{y}(t) \tag{28}$$

Using the modal transformation in Eq. (28), pre-multiplying Eq. (21) by $\mathbf{X}^T$ and using the orthogonality relationships in (27), equation of motion of a damped system in the modal coordinates may be obtained as

$$\ddot{y}(t) + X^T C X\dot{y}(t) + \Omega^2 y(t) = \tilde{f}(t) \tag{29}$$

Clearly, unless $\mathbf{X^T\,[C]\,X}$ is a diagonal matrix, no advantage can be gained by employing modal analysis because the equations of motion will still be coupled. To solve this problem, it is common to assume proportional damping. With the proportional damping assumption, the damping matrix [C] is simultaneously diagonalisable with [M] and [K]. This implies that the damping matrix in the modal coordinate

$$[\mathrm{C}'] = \mathrm{X}^{\mathrm{T}}[\mathrm{C}]\mathrm{X} \tag{30}$$

where [C′] is a diagonal matrix. This matrix is also known as the modal damping matrix. The damping factors ζ_j are defined from the diagonal elements of modal damping matrix as

$$C'_{jj} = 2\zeta_j\omega_j \quad \text{where} \quad j = 1,2,\ldots n \tag{31}$$

Such a damping model, introduced by Lord Rayleigh [43] is employed to analyse damped systems in the same manner as undamped systems since the equation of motion in the modal coordinates can be decoupled as

$$\ddot{y}_j(t) + 2\zeta_j\omega_j\dot{y}_j(t) + \omega_j^2 y(t) = \tilde{f}_j(t) \quad \text{where} \quad j = 1,2,\ldots n \tag{32}$$

The generalized proportional damping model expresses the damping matrix as a linear combination of the mass and stiffness matrices, that is

$$[C(\bar{\omega})] = \alpha_1[M(\bar{\omega})]\mathrm{f}([M^{-1}(\bar{\omega})][K(\bar{\omega})]) \tag{33}$$

where $\alpha_1 = 0.005$ is constant damping factor.

The transfer function matrix of the system can be obtained as

$$\begin{aligned} H(i\omega)(\bar{\omega}) &= X[-\omega^2 I + 2i\omega\zeta\Omega + \Omega^2]^{-1}X^T \\ &= \sum_{j=1}^{n}\frac{X_j X_j^T}{-\omega^2 + 2i\omega\zeta_j\omega_j + \omega_j^2} \end{aligned} \tag{34}$$

Using this, the dynamic response in the frequency domain with zero initial conditions can be conveniently represented as

$$\bar{\delta}(i\omega)(\bar{\omega}) = H(i\omega)\bar{f}(i\omega) = \sum_{j=1}^{n}\frac{X_j^T\bar{f}(i\omega)}{-\omega^2 + 2i\omega\zeta_j\omega_j + \omega_j^2}X_j \tag{35}$$

Therefore, the dynamic response of proportionally damped system can be expressed as a linear combination of the undamped mode shapes.

3. Kriging surrogate model

In general, a surrogate is an approximation of the Input/Output (I/O) function that is implied by the underlying simulation model. Surrogate models are fitted to the I/O data produced by the experiment with the simulation model. This simulation model may be either deterministic or random (stochastic). The Kriging model initially developed in spatial statistics by Danie Gerhardus Krige and subsequently extended by Matheron [2] and Cressie [3]. Kriging is a Gaussian process based modelling method, which is compact and cost effective for computation. Kriging surrogate models are employed to fit the data those are obtained for larger experimental areas than the areas used in low order polynomial regression. Hence Kriging models are global rather than local wherein such models are used for prediction. In present study, Kriging model [6] for simulation of required output (say natural frequency) is expressed as,

$$y(x) = y_0(x) + Z(x) \tag{36}$$

where $y(x)$ is the unknown function of interest, x is an m dimensional vector (m design variables), $y_0(x)$ is the known approximation (usually polynomial) function and $Z(x)$ represents is the realization of a stochastic process with mean zero, variance, and nonzero covariance. In the model, the local deviation at an unknown point ($\mathbf{x}$) is expressed using stochastic processes. The sample points are interpolated with the Gaussian random function as the correlation function to estimate the trend of the stochastic processes. The $y_0(x)$ term is similar to a polynomial response surface, providing global model of the design space [44] (see Fig. 2)

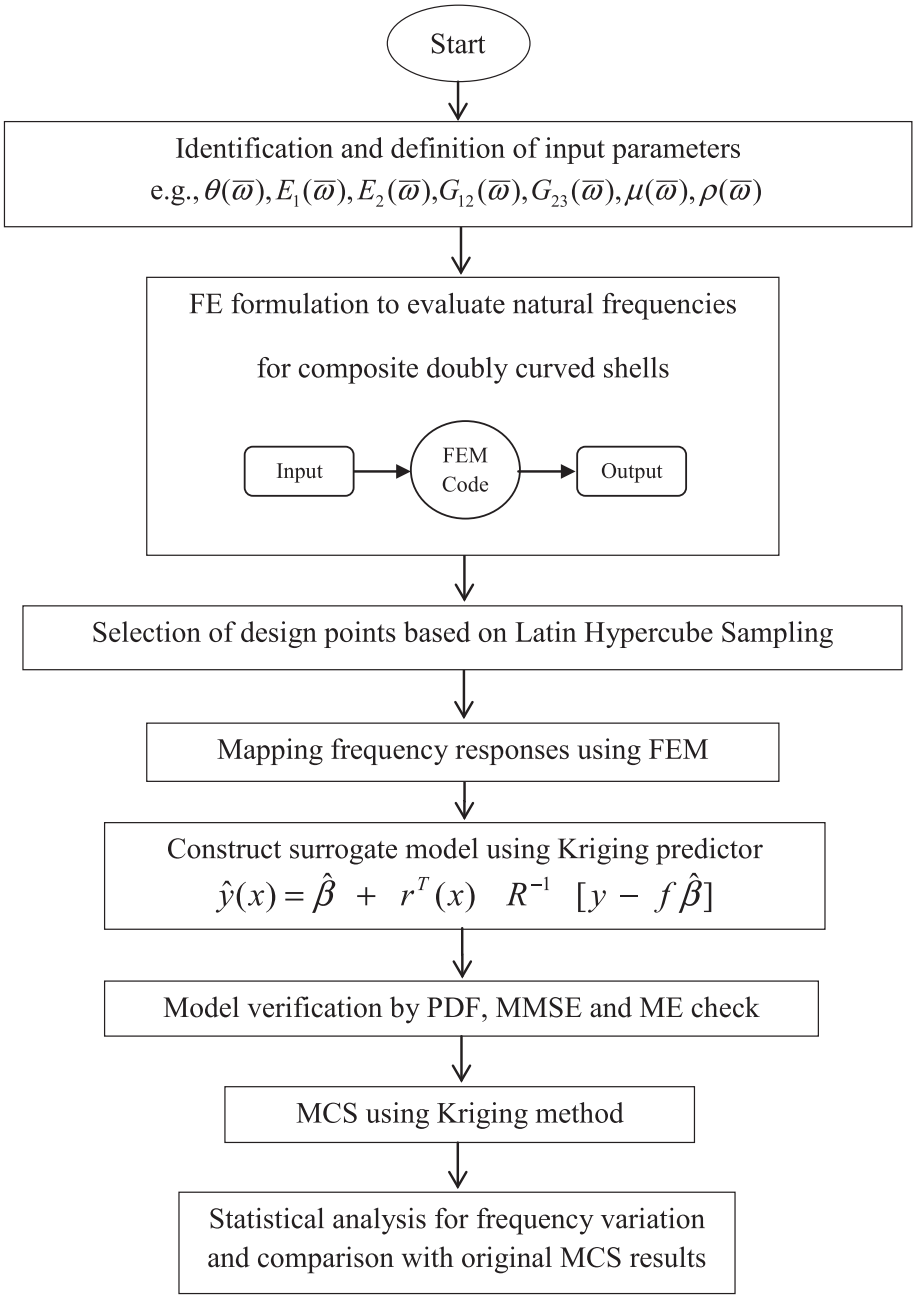

Fig. 3. Flowchart of stochastic natural frequency analysis using Kriging model.

Table 1
Non-dimensional fundamental natural frequencies [$\omega = \omega_n L^2 \sqrt{(\rho/E_1 h^2)}$] of three layered [$\theta/-\theta/\theta$] graphite–epoxy twisted plates, $L/b = 1$, $b/h = 20$, $\psi = 30°$.

Ply-orientation angle, θ (°)	Present FEM					Qatu and Leissa [47]
	4×4	6×6	8×8	10×10	12×12	
15	0.8588	0.8618	0.8591	0.8543	0.8540	0.8759
30	0.6753	0.6970	0.6752	0.6722	0.6717	0.6923
45	0.4691	0.4732	0.4698	0.4578	0.4575	0.4831
60	0.3189	0.3234	0.3194	0.3114	0.3111	0.3283

Table 2
Convergence study for maximum mean square error (MMSE) and maximum error (in percentage) using Kriging model compared to original MCS with different sample sizes for combined variation of 28 nos. input parameters of graphite–epoxy angle-ply (45°/−45°/−45°/45°) composite cantilever spherical shells, considering $E_1 = 138$ GPa, $E_2 = 8.9$ GPa, $G_{12} = G_{13} = 7.1$ GPa, $G_{23} = 2.84$ GPa, $t = 0.005$ m, $\mu = 0.3$.

Sample size	Parameter	Fundamental natural frequency	Second natural frequency	Third natural frequency
450	MMSE	0.0289	0.1968	0.2312
	Max error (%)	2.4804	7.6361	6.5505
500	MMSE	0.0178	0.1466	0.2320
	Max error (%)	1.6045	2.6552	3.0361
550	MMSE	0.0213	0.1460	0.2400
	Max error (%)	1.2345	2.0287	1.8922
575	MMSE	0.0207	0.1233	0.2262
	Max error (%)	1.1470	1.8461	1.7785
600	MMSE	0.0177	0.1035	0.2071
	Max error (%)	1.1360	1.7208	1.7820
625	MMSE	0.0158	0.0986	0.1801
	Max error (%)	1.0530	1.7301	1.6121
650	MMSE	0.0153	0.0966	0.1755
	Max error (%)	0.9965	1.8332	1.6475

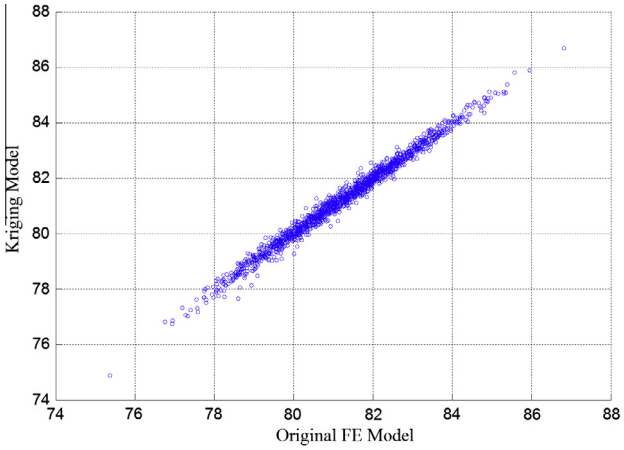

Fig. 4. Scatter plot for Kriging model with respect to original FE model of fundamental natural frequency for combined variation of ply orientation angle [$\theta(\bar{\omega})$], longitudinal elastic modulus [$E_1(\bar{\omega})$], transverse elastic modulus [$E_2(\bar{\omega})$], longitudinal shear modulus [$G_{12}(\bar{\omega})$], Transverse shear modulus [$G_{23}(\bar{\omega})$], Poisson's ratio [$\mu(\bar{\omega})$] and mass density [$\rho(\bar{\omega})$] for composite cantilevered spherical shells, considering sample size = 10,000, $E_1 = 138$ GPa, $E_2 = 8.9$ GPa, $G_{12} = G_{13} = 7.1$ GPa, $G_{23} = 2.84$ GPa, $\rho = 3202$ kg/m^3, $t = 0.005$ m, $\mu = 0.3$.

In present study, $y_0(x)$ globally approximates the design space, $Z(x)$ creates the localized deviations so that the Kriging model interpolates the p-sampled data points for composite shallow doubly curved shells; however, non-interpolative Kriging models can also be created to smooth noisy data [3]. The covariance matrix of $Z(x)$ is given as

$$Cov[Z(x^i), Z(x^j)] = \sigma^2 R[R(x^i, x^j)] \tag{37}$$

where R is a $(p \times p)$ correlation matrix and $R(\boldsymbol{x}^i, \boldsymbol{x}^j)$ is the correlation function between any two of the p-sampled data points x^i and x^j. R is an $(p \times p)$ symmetric matrix with ones along the diagonal. The correlation function $R(x^i, x^j)$ is specified by the user, and a variety of correlation functions exist. Using Gaussian correlation function

$$R(x^i, x^j) = \exp\left[-\sum_{k=1}^{n} \theta_k |x_k^i - x_k^j|^2\right] \tag{38}$$

where n is the number of design variables, θ_k is the unknown correlation parameters used to fit the model, and x_k^i and x_k^j are the k-th components of the sample points x^i and x^j, respectively. The predicted estimates, $\hat{y}$ of the response $y(x)$ at random values of x are defined as Kriging predictor

$$\hat{y}(x) = \hat{\beta} + r^T(x) R^{-1}[y - f\hat{\beta}] \tag{39}$$

where y is the column vector of length p that contains the sample values of the frequency responses and f is a column vector of length p that is filled with ones when $y_0(x)$ is taken as constant. Now, $r^T(x)$ is the correlation vector of length p between the random x and the sample data points $\{x^1, x^2, \ldots x^p\}$

$$r^T(x) = [R(x, x^1), R(x, x^2), R(x, x^3) \ldots R(x, x^p)]^T \tag{40}$$

$$\hat{\beta} = (f^T R^{-1} f)^{-1} f^T R^{-1} y \tag{41}$$

An estimate of the variance between underlying global model $\hat{\beta}$ and y is estimated by

$$\hat{\sigma}^2 = \frac{1}{p}(y - f\hat{\beta})^T R^{-1}(y - f\hat{\beta}) \tag{42}$$

Now the model fitting is accomplished by maximum likelihood (i.e., best guesses) for θ_k. The maximum likelihood estimates (i.e., "best guesses") for the θ_k in Eq. (35) used to fit a Kriging model are obtained as

$$Max \cdot \Gamma(\theta_k) = -\frac{1}{2}[p \ln(\hat{\sigma}^2) + \ln|R|] \tag{43}$$

where the variance σ^2 and $|R|$ are both functions of θ_k, is solved for positive values of θ_k as optimization variables. After obtaining

Table 3
Non-dimensional fundamental frequencies $\left[\omega = \omega_n a^2 \sqrt{\frac{12\rho(1-\mu^2)}{E_1 t^2}}\right]$ of isotropic, corner point-supported spherical and hyperbolic paraboloidal shells considering $a/b = 1$, $a'/a = 1$, $a/t = 100$, $a/R = 0.5$, $\mu = 0.3$.

R_x/R_y	Shell type	Present FEM	Leissa and Narita [48]	Chakravorty et al. [39]
1	Spherical	50.74	50.68	50.76
−1	Hyperbolic paraboloid	17.22	17.16	17.25

Kriging based surrogate, the random process $Z(x)$ provides the approximation error that can be used for improving the surrogate model. The maximum mean square error (MMSE) and maximum error (ME) are calculated as,

$$\text{MMSE} = max \cdot \left[\frac{1}{k}\sum_{i=1}^{k}(\bar{y}_i - y_i)^2\right] \tag{44}$$

$$\text{ME}\ (\%) = Max\left[\frac{y_{i,MCS} - y_{i,Kriging}}{Y_{i,MCS}}\right] \tag{45}$$

where y_i and $\bar{y}_i$ are the vector of the true values and the vector corresponding to i-th prediction, respectively.

4. Stochastic approach using Kriging model

The stochasticity in material properties of laminated composite shallow doubly curved shells, such as longitudinal elastic modulus, transverse elastic modulus, longitudinal shear modulus, transverse shear modulus, Poisson's ratio, mass density and geometric properties such as ply-orientation angle as input parameters are considered for natural frequency analysis of composite shallow doubly curved shells. In the present study, frequency domain feature (first three natural frequencies) is considered as output. It is assumed that the distribution of randomness of input parameters exists within a certain band of tolerance with their central deterministic mean values. Therefore the normal distribution considered is expressed as

$$f(x) = \frac{1}{\sigma\sqrt{2\pi}}\exp\left[-\frac{1}{2}\left(\frac{x-\bar{x}}{\sigma}\right)^2\right] \tag{46}$$

where σ^2 is the variance of the random variable; $\bar{x}$ is the mean of the random variable. The cases wherein the random variables considered in each layer of laminate are investigated for

(a) Variation of ply-orientation angle only: $\theta(\bar{\omega}) = \{\theta_1\theta_2\theta_3 \ldots \theta_i \ldots \theta_l\}$.
(b) Variation of longitudinal elastic modulus only: $E_1(\bar{\omega}) = \{E_{1(1)}E_{1(2)}E_{1(3)} \ldots E_{1(i)} \ldots E_{1(l)}\}$.
(c) Variation of transverse elastic modulus only: $E_2(\bar{\omega}) = \{E_{2(1)}E_{2(2)}E_{2(3)} \ldots E_{2(i)} \ldots E_{2(l)}\}$.
(d) Variation of longitudinal shear modulus only: $G_{12}(\bar{\omega}) = \{G_{12(1)}G_{12(2)}G_{12(3)} \ldots G_{12(i)} \ldots G_{12(l)}\}$.
(e) Variation of transverse shear modulus only: $G_{23}(\bar{\omega}) = \{G_{23(1)}G_{23(2)}G_{23(3)} \ldots G_{23(i)} \ldots G_{23(l)}\}$.
(f) Variation of Poisson's ratio only: $\mu(\bar{\omega}) = \{\mu_1\mu_2\mu_3 \ldots \mu_i \ldots \mu_l\}$.
(g) Variation of mass density only: $\rho(\bar{\omega}) = \{\rho_1\rho_2\rho_3 \ldots \rho_i \ldots \rho_l\}$.

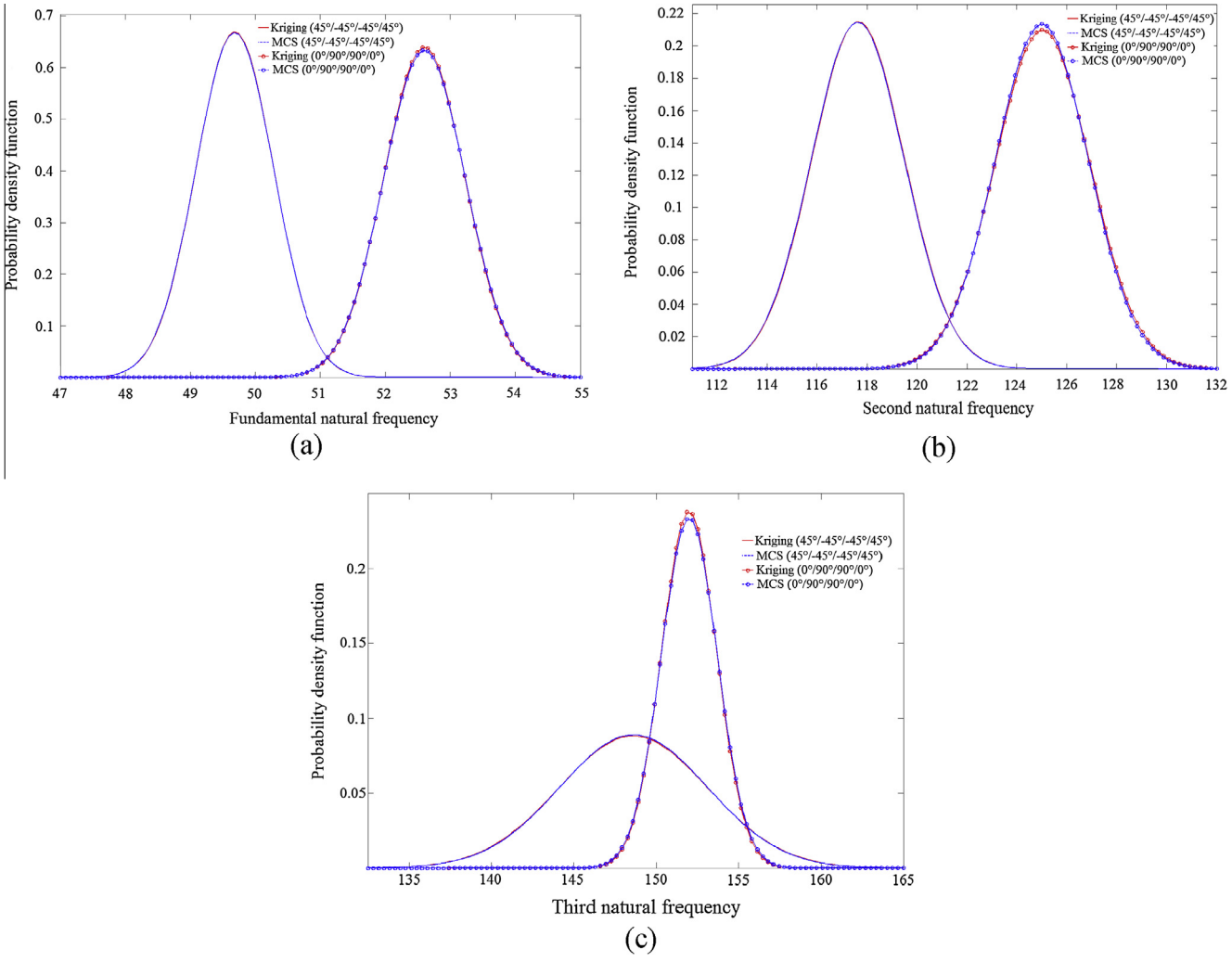

Fig. 5. (a–c) Probability density function obtained by original MCS and Kriging model with respect to first three natural frequencies for individual variation of ply orientation angle $[\theta(\bar{\omega})]$ for composite elliptical paraboloid shells, considering sample size = 10,000, $R_x \neq R_y$, $R_{xy} = \alpha$, E_1 = 138 GPa, E_2 = 8.9 GPa, $G_{12} = G_{13}$ = 7.1 GPa, G_{23} = 2.84 GPa, ρ = 3202 kg/m^3, t = 0.005 m, μ = 0.3.

(h) Combined variation of ply orientation angle, elastic modulus (longitudinal and transverse), shear modulus (longitudinal and transverse), Poisson's ratio and mass density.

$$g\{\theta(\bar{\omega}),\rho(\bar{\omega}),G_{12}(\bar{\omega}),G_{23}(\bar{\omega}),E_1(\bar{\omega})\} = \{\Phi_1(\theta_1 \dots \theta_l),\Phi_2(E_{1(1)} \dots E_{1(l)}),\Phi_3(E_{2(1)} \dots E_{2(l)}),\Phi_4(G_{12(1)} \dots G_{12(l)}),\Phi_5(G_{23(1)} \dots G_{23(l)}),\Phi_6(\mu_1 \dots \mu_l),\Phi_7(\rho_1 \dots \rho_l)\}$$

where θ_i, $E_{1(i)}$, $E_{2(i)}$, $G_{12(i)}$, $G_{23(i)}$, μ_i and ρ_i are the ply orientation angle, elastic modulus along longitudinal and transverse direction, shear modulus along longitudinal direction, shear modulus along transverse direction, Poisson's ratio and mass density, respectively and 'l' denotes the number of layer in the laminate. In present study, $\pm 10^\circ$ for ply orientation angle with subsequent ±10% tolerance for material properties from deterministic mean value are considered. Latin hypercube sampling [45] is employed for generating sample points to ensure the representation of all portions of the vector space. In Latin hypercube sampling, the interval of each dimension is divided into m non-overlapping intervals having equal probability considering a uniform distribution, so the intervals should have equal size. Moreover, the sample is chosen randomly from a uniform distribution a point in each interval in each dimension and the random pair is selected considering equal likely combinations for the point from each dimension (see Fig. 3).

5. Results and discussion

In the present study, four layered graphite–epoxy symmetric angle-ply and cross-ply laminated composite cantilever shallow doubly curved shells namely spherical ($R_x/R_y = 1$), hyperbolic paraboloid ($R_x/R_y = -1$) and elliptical paraboloid ($R_x/R_y \neq 1$) are considered. The length, width and thickness of the composite laminate considered in the present analysis are 1 m, 1 mm and 5 mm, respectively. Material properties of graphite–epoxy composite [46] considered with deterministic mean value as $E_1 = 138.0$ GPa, $E_2 = 8.96$ GPa, $G_{12} = 7.1$ GPa, $G_{13} = 7.1$ GPa, $G_{23} = 2.84$ GPa, $\mu = 0.3$, $\rho = 3202$ kg/m^3. A typical discretization of (6×6) mesh on plan area with 36 elements 133 nodes with natural coordinates of an isoparametric quadratic plate bending element are considered for the present FEM approach. For full scale MCS, number of original FE analysis is same as the sampling size. In general for complex composite structures, the performance function is not available as an explicit function of the random design variables. The random response in terms of natural frequencies of the composite structure can only be evaluated numerically at the end of a structural

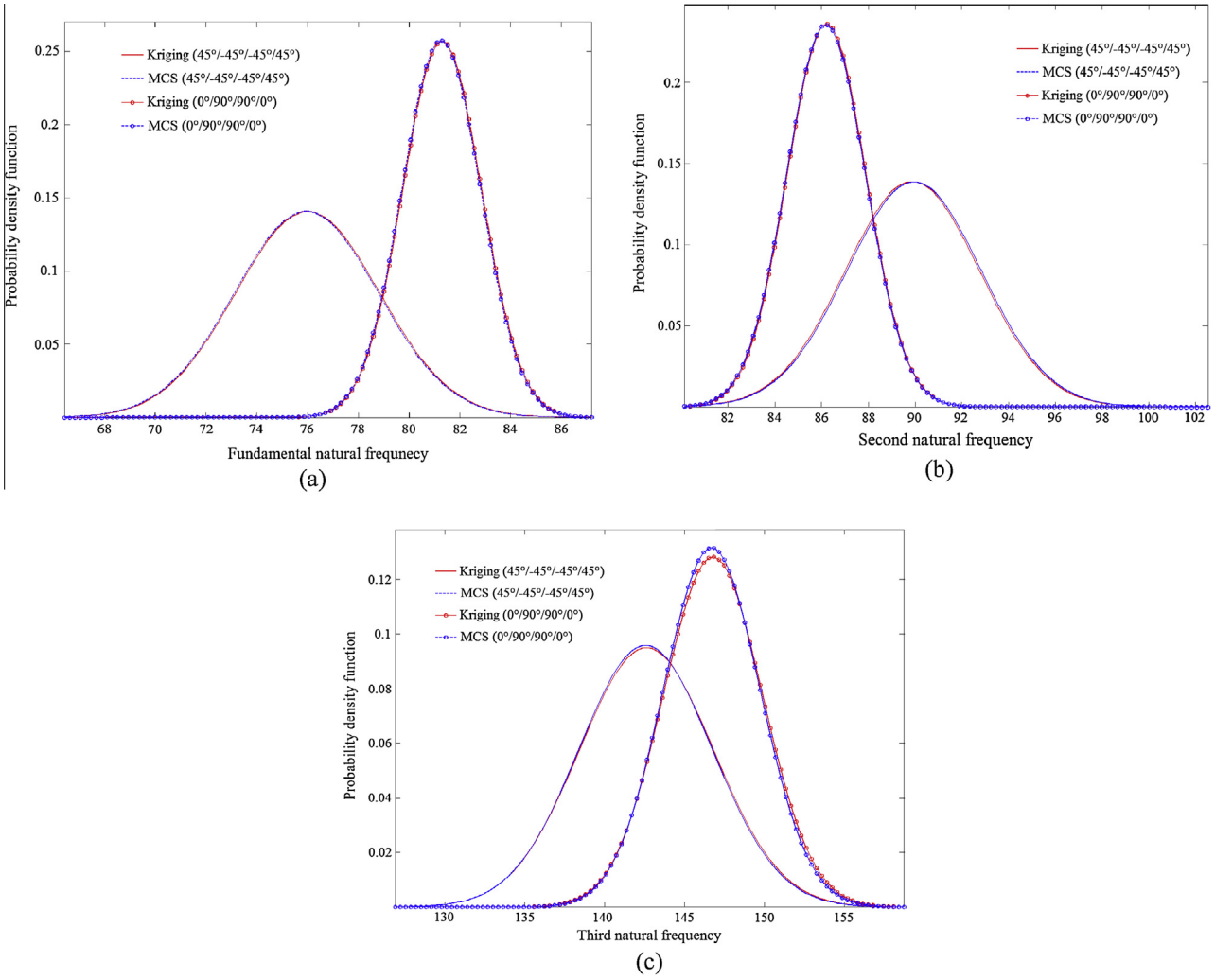

Fig. 6. (a–c) Probability density function obtained by original MCS and Kriging model with respect to first three natural frequencies for combined variation of ply orientation angle [$\theta(\bar{\omega})$], mass density [$\rho(\bar{\omega})$], longitudinal shear modulus [$G_{12}(\bar{\omega})$], transverse shear modulus [$G_{23}(\bar{\omega})$] and longitudinal elastic modulus [$E_1(\bar{\omega})$] and transverse elastic modulus [$E_2(\bar{\omega})$] for composite spherical shells, considering sample size = 10,000, $E_1 = 138$ GPa, $E_2 = 8.9$ GPa, $G_{12} = G_{13} = 7.1$ GPa, $G_{23} = 2.84$ GPa, $\rho = 3202$ kg/m^3, $t = 0.005$ m, $\mu = 0.3$.

Table 4
Individual stochasticity of $[\theta(\bar{\omega}), E_1(\bar{\omega}), E_2(\bar{\omega}), G_{12}(\bar{\omega}), G_{23}(\bar{\omega}), \mu(\bar{\omega}), \rho(\bar{\omega})]$ for angle-ply (45°/−45°/−45°/45°) composite shells.

Type	Value	$\theta(\bar{\omega})$			$E_1(\bar{\omega})$			$E_2(\bar{\omega})$			$G_{12}(\bar{\omega})$			$G_{23}(\bar{\omega})$			$\mu(\bar{\omega})$			$\rho(\bar{\omega})$		
		f_1	f_2	f_3	f_1	f_2	f_3	f_1	f_2	f_3	f_1	f_2	f_3	f_1	f_2	f_3	f_1	f_2	f_3	f_1	f_2	f_3
SP	Min.	69.76	85.06	134.58	73.94	88.29	139.32	68.75	78.21	127.40	78.12	92.90	147.12	75.37	90.75	142.28	75.36	90.71	142.23	72.31	87.06	136.50
	Max.	84.04	97.52	154.33	76.69	93.03	145.01	69.64	79.68	128.99	81.89	95.89	153.71	75.39	90.77	142.33	75.40	90.81	142.38	78.95	95.06	149.04
	Mean	76.44	90.55	144.10	75.35	90.71	142.26	69.21	78.97	128.22	80.06	94.45	150.51	75.38	90.76	142.30	75.38	90.76	142.30	75.41	90.79	142.35
	SD	2.57	2.32	3.53	0.46	0.86	1.01	0.17	0.28	0.30	0.62	0.50	1.09	0.00	0.00	0.01	0.01	0.02	0.03	1.09	1.31	2.06
HP	Min.	27.79	105.54	156.30	27.66	105.87	160.10	28.16	107.87	163.27	28.95	110.74	168.32	28.34	108.55	163.78	28.33	108.54	163.79	27.19	104.15	157.16
	Max.	29.28	113.02	171.42	28.98	111.10	167.29	28.52	109.27	164.40	29.84	113.80	174.47	28.35	108.60	163.89	28.35	108.62	163.89	29.68	113.72	171.60
	Mean	28.40	108.68	164.52	28.33	108.53	163.77	28.34	108.58	163.84	29.41	112.32	171.49	28.34	108.58	163.84	28.34	108.58	163.84	28.35	108.62	163.89
	SD	0.21	1.26	2.79	0.22	0.86	1.19	0.07	0.28	0.22	0.15	0.51	1.02	0.00	0.01	0.02	0.00	0.01	0.02	0.41	1.57	2.37
EP	Min.	47.94	113.17	136.05	48.29	114.07	144.13	49.13	116.48	146.49	48.35	114.61	143.00	49.33	116.84	146.77	49.31	116.78	146.73	47.33	112.09	140.81
	Max.	51.93	123.91	160.73	50.32	119.42	149.16	49.54	117.22	147.10	50.25	118.94	150.28	49.34	116.86	146.82	49.36	116.93	146.87	51.67	122.38	153.75
	Mean	49.68	117.65	148.61	49.32	116.81	146.75	49.34	116.85	146.80	49.33	116.84	146.77	49.34	116.85	146.80	49.34	116.85	146.80	49.35	116.89	146.85
	SD	0.60	1.85	4.52	0.33	0.94	0.87	0.08	0.14	0.11	0.32	0.72	1.20	0.00	0.00	0.01	0.01	0.03	0.02	0.71	1.69	2.12

Table 5
Individual stochasticity of $[\theta(\bar{\omega}), E_1(\bar{\omega}), E_2(\bar{\omega}), G_{12}(\bar{\omega}), G_{23}(\bar{\omega}), \mu(\bar{\omega}), \rho(\bar{\omega})]$ for cross-ply (0°/90°/90°/0°) composite shells.

Type	Value	$\theta(\bar{\omega})$			$E_1(\bar{\omega})$			$E_2(\bar{\omega})$			$G_{12}(\bar{\omega})$			$G_{23}(\bar{\omega})$			$\mu(\bar{\omega})$			$\rho(\bar{\omega})$		
		f_1	f_2	f_3	f_1	f_2	f_3	f_1	f_2	f_3	f_1	f_2	f_3	f_1	f_2	f_3	f_1	f_2	f_3	f_1	f_2	f_3
SP	Min.	78.96	84.43	139.11	80.16	84.35	145.68	75.20	90.49	142.01	83.47	88.44	151.38	82.61	86.96	150.42	82.59	86.94	150.40	79.25	83.42	144.31
	Max.	82.53	89.20	150.16	84.93	89.37	154.42	75.55	91.02	142.59	84.76	90.47	152.73	82.63	86.98	150.47	82.65	87.00	150.50	86.53	91.09	157.57
	Mean	81.76	86.82	148.23	82.59	86.94	150.23	75.38	90.76	142.30	84.13	89.50	152.08	82.62	86.97	150.44	82.62	86.97	150.44	82.65	87.00	150.49
	SD	0.57	0.64	1.63	0.79	0.89	1.56	0.06	0.10	0.11	0.23	0.34	0.23	0.00	0.00	0.01	0.01	0.01	0.02	1.19	1.26	2.18
HP	Min.	28.72	106.04	159.86	29.30	107.46	169.47	29.94	109.69	173.71	30.58	112.47	176.93	30.16	110.35	174.71	30.15	110.31	174.69	28.93	105.87	167.66
	Max.	31.31	114.45	179.15	30.98	113.12	179.77	30.37	111.01	175.77	31.20	115.55	179.98	30.17	110.38	174.84	30.17	110.42	174.87	31.59	115.59	183.06
	Mean	30.03	110.29	173.55	30.15	110.32	174.71	30.16	110.37	174.78	30.89	114.02	178.47	30.16	110.37	174.78	30.16	110.37	174.78	30.17	110.40	174.84
	SD	0.49	1.56	3.14	0.28	0.93	1.71	0.08	0.25	0.38	0.11	0.53	0.54	0.00	0.01	0.02	0.00	0.02	0.03	0.44	1.60	2.53
EP	Min.	50.66	117.30	145.55	51.36	121.84	148.60	52.53	124.79	151.88	52.43	124.16	151.73	52.91	125.50	153.03	52.91	125.46	153.02	50.76	120.41	146.84
	Max.	54.25	129.67	155.85	54.45	129.08	157.49	53.29	126.19	154.14	53.38	126.80	154.25	52.92	125.54	153.12	52.93	125.58	153.13	55.42	131.47	160.32
	Mean	52.60	125.03	151.99	52.90	125.48	152.96	52.92	125.52	153.07	52.91	125.51	153.06	52.92	125.52	153.07	52.92	125.52	153.07	52.94	125.56	153.13
	SD	0.62	1.90	1.67	0.49	1.22	1.43	0.14	0.25	0.44	0.16	0.43	0.43	0.00	0.01	0.02	0.00	0.03	0.02	0.77	1.82	2.21

analysis procedure such as the finite element method which is often time-consuming. The present Kriging method is employed to find a predictive and representative surrogate model relating each natural frequency to a number of input variables. The Kriging surrogate models are used to determine the first three natural frequencies corresponding to given values of input variables, instead of time-consuming deterministic FE analysis. The surrogate model thus represents the result of the structural analysis encompassing every possible combination of all input variables. From this, thousands of combinations of all design variables can be created and performed a pseudo analysis for each variable set, by simply adopting the corresponding predictive values. The probability density function (PDF) is plotted as the benchmark of bottom line results. Due to paucity of space, only a few important representative results are furnished.

5.1. Validation

The present computer code is validated with the results available in the open literature. Table 1 presents the non-dimensional fundamental frequencies of graphite–epoxy composite twisted plates with different ply-orientation angle [47]. Convergence studies are performed using mesh division of (4×4), (6×6), (8×8), (10×10) and (12×12) wherein (6×6) mesh is found to provide best results with the least difference compared to benchmarking results [47]. The differences between the results by Qatu and Leissa [47] and the present finite element approach can be attributed to consideration of transverse shear deformation and rotary inertia and also to the fact that Ritz method overestimates the structural stiffness of the composite plates. Hence, the lower mesh size (6×6) is employed in the present analysis due to computational efficiency. Another convergence study is carried out for selection of sample size with respect to maximum mean square error (MMSE) and maximum error (in percentage) using Kriging method compared to original MCS (10,000 samples) with respect to variation of only ply-orientation angle in each layer of graphite–epoxy angle-ply (45°/−45°/−45°/45°) composite cantilever spherical shells as furnished in Table 2. To optimize the computation time in conjunction with MMSE and ME, a sample size of 625 is chosen for combined variation of twenty-eight (28) input parameters for the present study. In contrast, a sample size of 30 is chosen in the similar fashion for individual random variation with four (04) input parameters for the present study. Table 3 represents the non-dimensional fundamental frequencies of isotropic, corner point-supported spherical and hyperbolic paraboloid shells [39,48]. All these studies depict an excellent agreement and hence it demonstrates the capability of the computer codes developed and insures the accuracy of analyses. Fig. 4 depicts a representative plot describing the relationship between the original FE model and the constructed Kriging model for fundamental natural frequencies signifying the accuracy of the present Kriging model. A comparative study addressing the probability density functions (PDF) for both original MCS and Kriging model using sample size of 10,000 is carried out corresponding to first three natural frequencies with typical laminated shell configuration as furnished in Fig. 5 (individual variation of ply orientation angle) and Fig. 6 (combined random variation of parameters). The low scatterness of the points found around the diagonal line in Fig. 4 and the low deviation obtained between the probability distribution function estimations of original MCS and Kriging responses in Figs. 5 and 6 corroborate the fact that the present surrogate models are accurately formed. These two plots are checked for all other cases and are found in good agreement ensuring the efficiency and accuracy of the constructed Kriging models. While evaluating the statistics of responses through full scale MCS, computational time is exorbitantly high because it involves number of repeated FE analysis. However, in the present method, MCS is conducted in conjunction with Kriging model. Here, although the same sampling size as in direct MCS (with sample size of 10,000) is considered, the number of original FE analysis is much less compared to direct MCS and is equal to number of samples required to construct the Kriging surrogate model. Hence, the computational time and effort expressed in terms of FE calculation is reduced compared to full scale direct MCS. This provides an efficient affordable way for simulating the uncertainties in natural frequency.

5.2. Statistical analysis

The variation of material properties like elastic modulus (longitudinal and transverse) $[E_1(\bar{\omega}), E_2(\bar{\omega})]$, shear modulus (longitudinal and transverse) $[G_{12}(\bar{\omega}), G_{23}(\bar{\omega})]$, Poisson's ratio $[\mu(\bar{\omega})]$ and mass density $[\rho(\bar{\omega})]$ considered in each layer of the composite shallow doubly curved shells are scaled randomly in the range having the lower and the upper limit as ±10% variability with respective mean values while for ply orientation angle $[\theta(\bar{\omega})]$ the bound is considered as within ±10° fluctuation with respective

Table 6
Maximum value, minimum value, mean value and standard deviation (SD) using Kriging model for first three natural frequencies obtained due to combined stochasticity $[\theta(\bar{\omega}), E_1(\bar{\omega}), E_2(\bar{\omega}), G_{12}(\bar{\omega}), G_{23}(\bar{\omega}), \mu(\bar{\omega}), \rho(\bar{\omega})]$ for graphite–epoxy angle-ply (45°/−45°/-45°/45°) and cross-ply (0°/90°/90°/0°) composite shallow doubly curved shells considering E_1 = 138 GPa, E_2 = 8.9 GPa, $G_{12} = G_{13}$ = 7.1 GPa, G_{23} = 2.84 GPa, ρ = 3202 kg/m^3, t = 0.005 m, μ = 0.3.

Shell type	Values	Angle-ply (45°/−45°/−45°/45°)			Cross-ply (0°/90°/90°/0°)		
		Fundamental natural frequency	Second natural frequency	Third natural frequency	Fundamental natural frequency	Second natural frequency	Third natural frequency
Spherical (SP)	Min. value	67.81	81.14	129.79	75.46	80.55	133.98
	Max. value	86.15	101.39	156.77	86.99	91.71	158.45
	Mean value	75.98	89.96	142.61	81.31	86.21	146.79
	Standard deviation	2.82	2.86	4.15	1.55	1.69	3.11
Hyperbolic paraboloid (HP)	Min. value	26.46	100.86	149.01	27.38	100.54	151.89
	Max. value	30.53	117.66	174.55	32.26	118.04	184.67
	Mean value	28.16	107.62	162.00	29.76	109.37	170.69
	Standard deviation	0.54	2.26	3.77	0.71	2.47	4.29
Elliptical paraboloid (EP)	Min. value	45.97	108.11	128.37	48.20	112.48	138.22
	Max. value	53.22	127.70	163.86	56.46	135.33	160.86
	Mean value	49.34	116.89	147.24	52.35	123.97	149.81
	Standard deviation	1.04	2.79	4.91	1.14	2.93	3.14

mean values of each layer of laminates. The Kriging surrogate models are formed to generate first three natural frequencies for angle-ply and cross-ply composite shallow doubly curved shells. The natural frequencies of tested angle-ply (45°/−45°/−45°/45°) laminate are found to be lower than that of the same for cross-ply (0°/90°/90°/0°) laminate irrespective of geometry of the shells and stochasticity considered in random input parameters. Tables 4 and 5 represent the maximum values, minimum values and standard deviation using Kriging model for first three natural frequencies obtained due to individual stochasticity of ply-orientation angle $[\theta(\bar{\omega})]$, elastic modulus (longitudinal and transverse) $[E_1(\bar{\omega}), E_2(\bar{\omega})]$, shear modulus (longitudinal and transverse) $[G_{12}(\bar{\omega}), G_{23}(\bar{\omega})]$, and Poisson's ratio $[\mu(\bar{\omega})]$, mass density $[\rho(\bar{\omega})]$ in each layer due to randomness considered for angle-ply and cross-ply composite cantilever shells, respectively. In general, for both angle-ply and cross-ply laminates with respect to individual variation of input parameters, the maximum and minimum of mean value for fundamental natural frequency is observed for spherical shells and hyperbolic paraboloid shells, respectively while the same is found to be intermediate for elliptical paraboloid shells. In contrast, the maximum and minimum of mean value for second natural frequency is observed for elliptical paraboloid shells and spherical shells, respectively while the same is found to be intermediate for hyperbolic paraboloid shells. Interestingly,

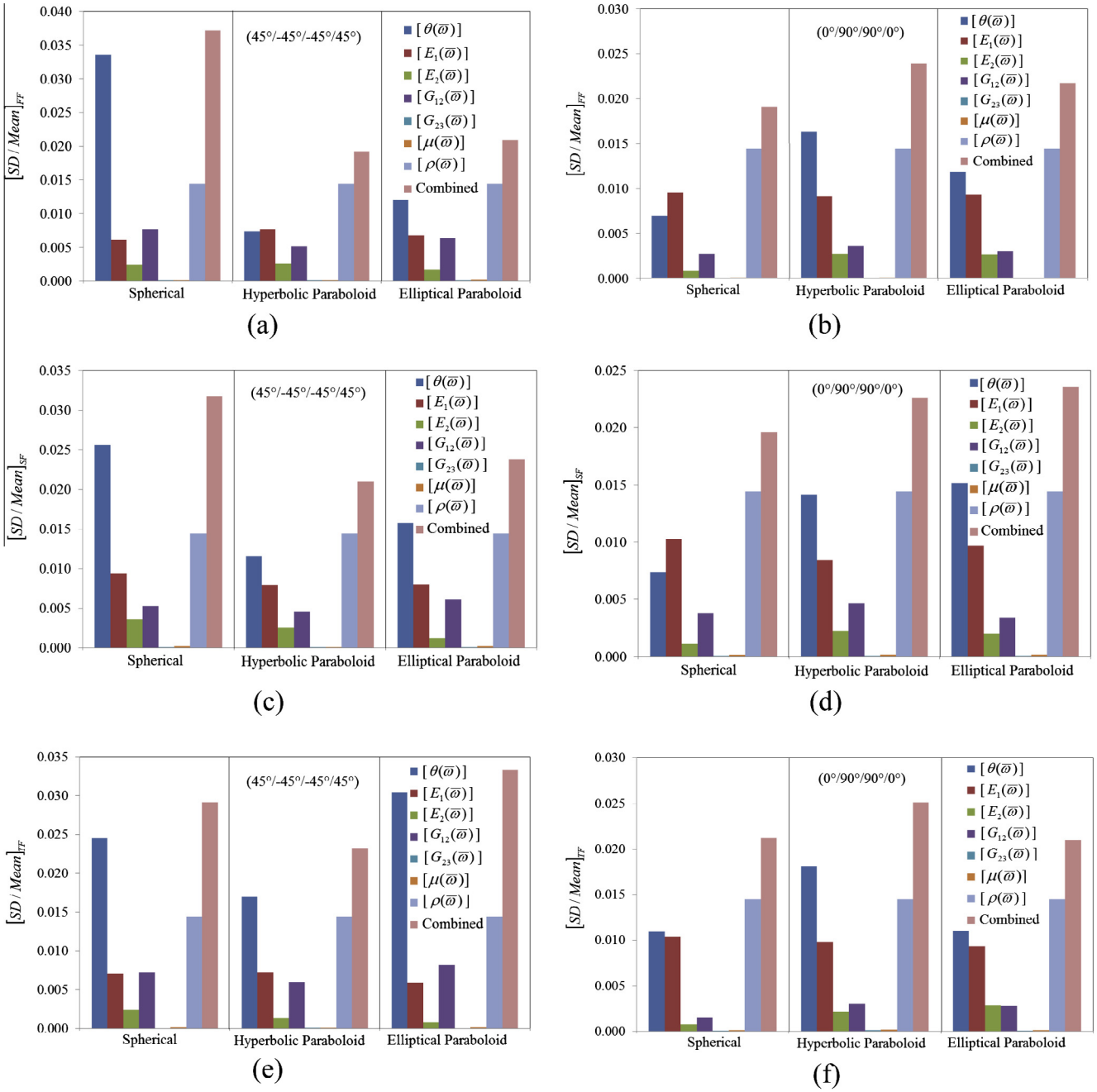

Fig. 7. [*SD*/*Mean*] of first three natural frequencies for individual variation of input parameters $[\theta(\bar{\omega})], [E_1(\bar{\omega})], [E_2(\bar{\omega})], [G_{12}(\bar{\omega})], [G_{23}(\bar{\omega})], [\mu(\bar{\omega})], [\rho(\bar{\omega})]$ and combined variation $[\theta(\bar{\omega}), E_1(\bar{\omega}), E_2(\bar{\omega}), G_{12}(\bar{\omega}), G_{23}(\bar{\omega}), \mu(\bar{\omega}), \rho(\bar{\omega})]$ for angle-ply (45°/−45°/−45°/45°) and cross-ply (0°/90°/90°/0°) composite shallow doubly curved shells (spherical, hyperbolic paraboloid and elliptical paraboloid), considering deterministic values as $E_1 = 138$ GPa, $E_2 = 8.9$ GPa, $G_{12} = G_{13} = 7.1$ GPa, $G_{23} = 2.84$ GPa, $\rho = 3202$ kg/m^3, $t = 0.005$ m, $\mu = 0.3$.

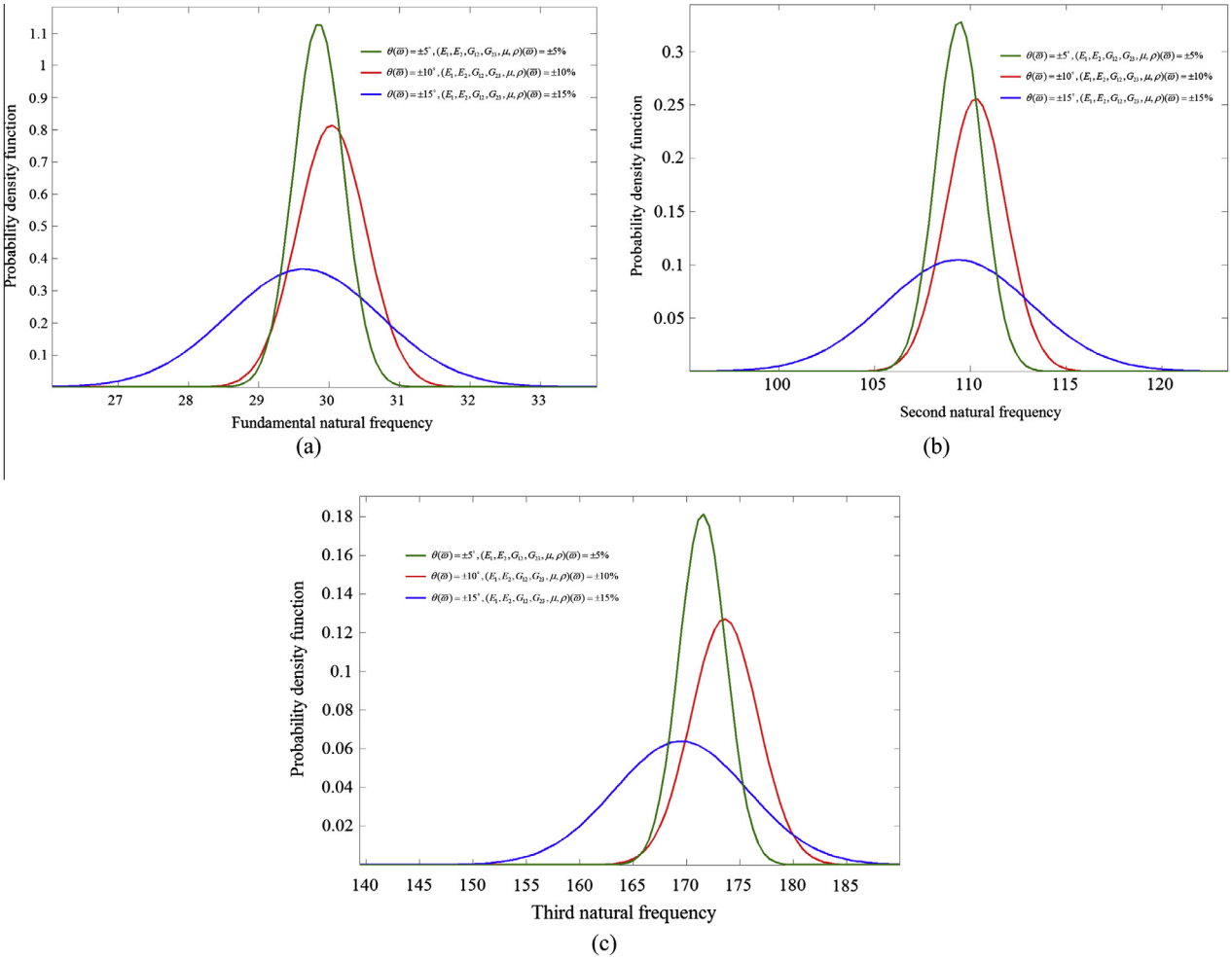

Fig. 8. Probability density function with respect to first three natural frequencies with different combined variation for cross-ply (0°/90°/90°/0°) composite hyperbolic paraboloid shallow doubly curved shells considering E_1 = 138 GPa, E_2 = 8.9 GPa, $G_{12} = G_{13}$ = 7.1 GPa, G_{23} = 2.84 GPa, ρ = 3202 kg/m^3, t = 0.005 m, μ = 0.3.

the maximum of mean value for third natural frequency is observed for hyperbolic paraboloid shells, trailed by elliptical paraboloid shells and the minimum mean value of third natural frequency is identified for spherical shells. Such variation in mean value of first three natural frequencies for three different types of shells can be attributed to the fact of predominance of geometric curvature effect which influences the elastic stiffness of the structure differently. Table 6 presents the maximum value, minimum value, mean value and standard deviation (SD) using Kriging model (625 samples) for first three natural frequencies obtained due to combined stochasticity $[\theta(\bar{\omega}), E_1(\bar{\omega}), E_2(\bar{\omega}), G_{12}(\bar{\omega}), G_{23}(\bar{\omega}),\ \mu(\bar{\omega}), \rho(\bar{\omega})]$ for graphite–epoxy angle-ply (45°/−45°/−45°/45°) and cross-ply (0°/90°/90°/0°) composite shallow doubly curved shells which as expected shows the maximum volatility compared to individual random variation in input parameter. Fig. 7 presents the [*SD*/*Mean*] of first three natural frequencies for individual variation of input parameters and combined variation for angle-ply (45°/−45°/−45°/45°) and cross-ply (0°/90°/90°/0°) composite shallow doubly curved shells. The degree of influence of ply-orientation angle $[\theta(\bar{\omega})]$ on tested natural frequencies is found to be maximum for spherical, hyperbolic paraboloid and elliptical paraboloid angle-ply composite laminate considering individual stochasticity of input parameters. In contrast, mass density $[\rho(\bar{\omega})]$ of spherical, hyperbolic paraboloid and elliptical paraboloid cross-ply composite laminate is identified to be most sensitive for first three natural frequencies while individual stochasticity of input parameters are considered. In both the cases of individual stochasticity, shear modulus along transverse direction $[G_{23}(\bar{\omega})]$ is observed to be least sensitive irrespective of type of shells. Due to cascading effect of variation of inputs in each layer of laminate, the combined variation of all input parameters is found to be most volatile for tested natural frequencies compared to individual input variations. The probability density function with respect to first three natural frequencies of combined variation for cross-ply (0°/90°/90°/0°) composite hyperbolic paraboloid shallow doubly curved shells considering ±5°, ±10° and ±15° for ply orientation angle with subsequent ±5%, ±10% and ±15% tolerance for material properties respectively from deterministic mean value are considered as furnished in Fig. 8. The representative stochastic mode-shapes for first three natural frequencies of angle-ply composite cantilever elliptical paraboloid shells are furnished in Fig. 9 wherein the first chordwise bending mode is observed corresponding to its fundamental natural frequency while the dominance of combined bending and torsion mode is found for second and third natural frequencies. It is also identified that the symmetry modes are absent and the nodal lines indicate with zero displacement amplitude. In the present study, a driving point and three cross points are considered to ascertain the corresponding amplitude (in dB) of frequency response function (FRF) wherein point 2 is considered as driving point while point 1, 3 and 4 are considered as the three cross response points as furnished in Fig. 1(b) assuming 0.5% damping factor for all the modes. A typical frequency

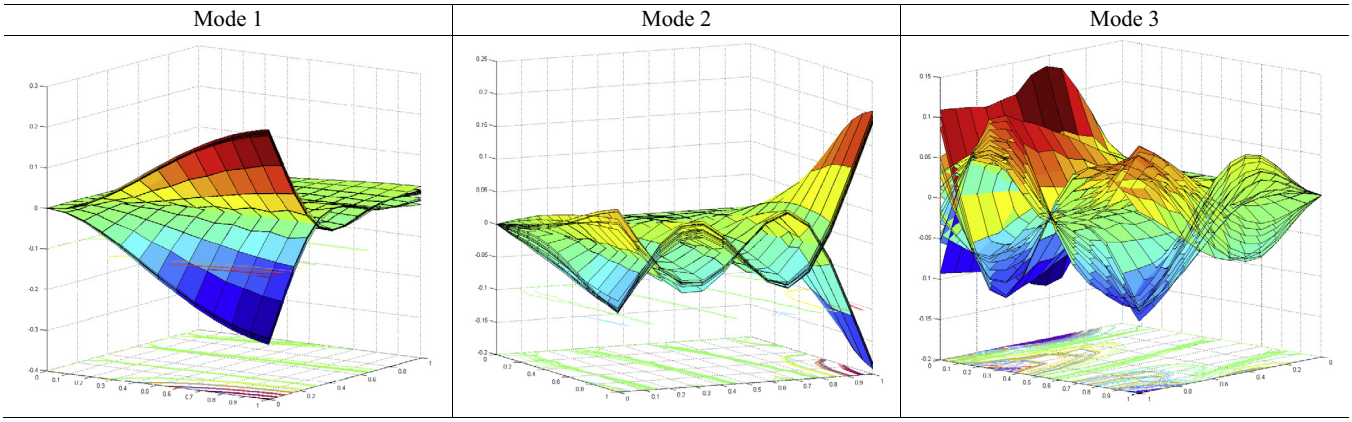

Fig. 9. Effect on modeshapes of first three modes due to combined stochasticity for four layered angle-ply (45°/−45°/−45°/45°) composite cantilever elliptical paraboloid shells considering E_1 = 138 GPa, E_2 = 8.9 GPa, $G_{12} = G_{13}$ = 7.1 GPa, G_{23} = 2.84 GPa, ρ = 3202 kg/m^3, t = 0.005 m, μ = 0.3.

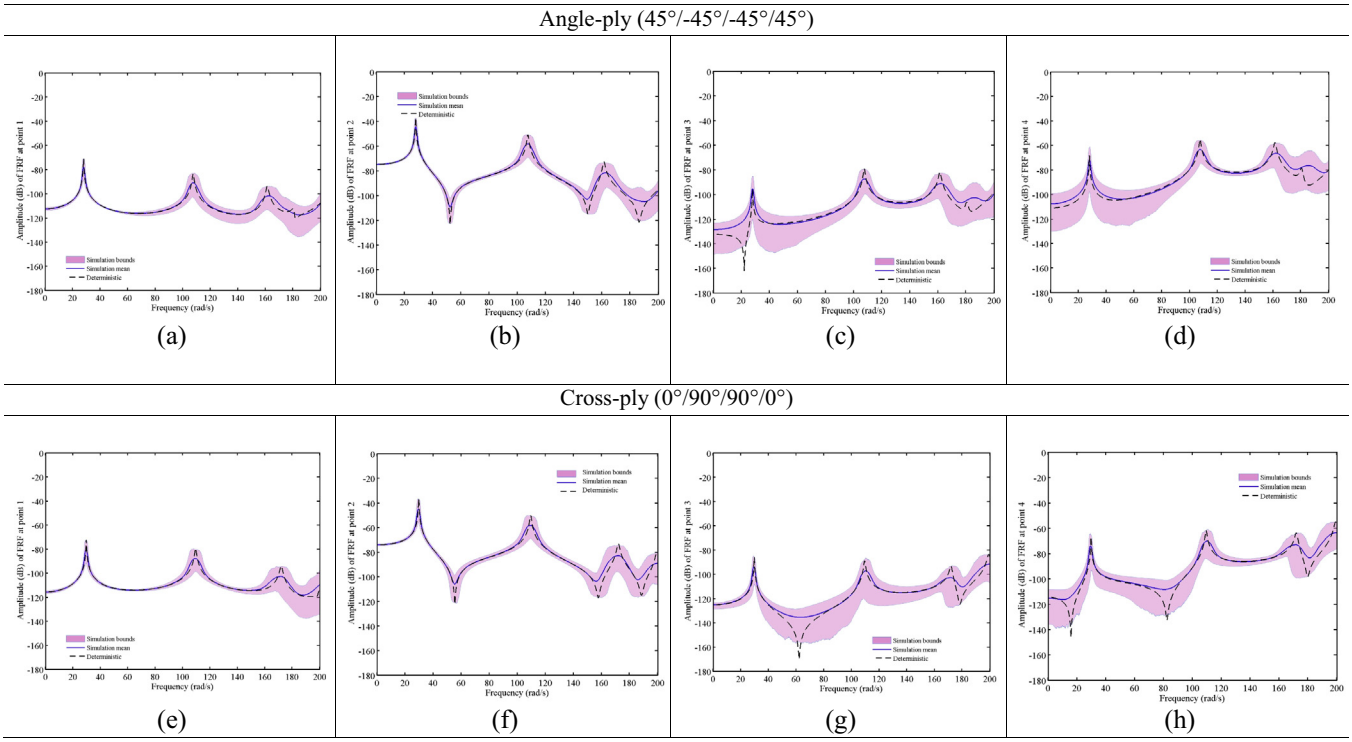

Fig. 10. Frequency response function (FRF) plot of simulation bounds, simulation mean and deterministic mean for combined stochasticity with four layered graphite epoxy composite cantilever elliptical paraboloid shells considering E_1 = 138 GPa, E_2 = 8.9 GPa, $G_{12} = G_{13}$ = 7.1 GPa, G_{23} = 2.84 GPa, ρ = 3202 kg/m^3, t = 0.005 m, μ = 0.3.

response function for combined variation $[\theta(\bar{\omega}), E_1(\bar{\omega}), E_2(\bar{\omega}), G_{12}(\bar{\omega}), G_{23}(\bar{\omega}), \mu(\bar{\omega}), \rho(\bar{\omega})]$ of both angle-ply (45°/−45°/−45°/45°) and cross-ply (0°/90°/90°/0°) composite cantilever elliptical paraboloid shells are furnished in Fig. 10. For a small amount of variability in input parameters, higher frequency shows wider volatility in simulation bounds of FRF compared to the same at lower frequency ranges. This can be attributed to the fact that due to multiplier effect at higher frequencies, a wider volatility of frequency response function is occurred.

6. Conclusions

The present study describes the random variable approach for propagation of uncertainty in natural frequency of angle-ply and cross-ply composite cantilever shallow doubly curved shells using Kriging model. The number of finite element analysis is reduced compared to original Monte Carlo simulation. It is observed that Kriging model can handle the large number of input parameters. The surrogate model formed from a small set of samples is found to establish the accuracy and computational efficacy. The results obtained by employing Kriging models are found accurate with the results found by using direct Monte Carlo simulation. The ply-orientation angle and mass density are found to be most sensitive among the tested input parameters while transverse shear modulus is identified as the least sensitive for first three natural frequencies. In general, for both angle-ply and cross-ply laminates with respect to individual variation of input parameters, the maximum and minimum of mean value for fundamental natural frequency is observed for spherical shells and hyperbolic paraboloid shells, respectively while the same is found to be intermediate

for elliptical paraboloid shells. The first chordwise bending mode is observed corresponding to its fundamental frequency while the dominance of combined bending and torsion mode is found for second and third natural frequencies, respectively. For a given amount of variability in the random input parameters, more volatility in the output quantities are observed in the higher frequency ranges compared to lower frequency ranges irrespective of frequency response function points. The future investigation will be carried out to interrogate whether the above conclusions hold true for more complex system.

References

[1] Cressie NAC. The origins of Kriging. Math Geol 1990;22:239–52.
[2] Matheron G. Principles of geostatistics. Econom Geol 1963;58(8):1246–66.
[3] Cressie NAC. Statistics for spatial data. Revised ed. New York: Wiley; 1993.
[4] Montgomery DC. Design and analysis of experiments. N.J.: J. Wiley and Sons; 1991.
[5] Michael JB, Norman RD. On minimum-point second-order designs. Technometrics 1974;16(4):613–6.
[6] Martin JD, Simpson TW. Use of Kriging models to approximate deterministic computer models. AIAA J 2005;43(4):853–63.
[7] Sakata S, Ashida F, Zako M. An efficient algorithm for Kriging approximation and optimization with large-scale sampling data. Comput Methods Appl Mech Eng 2004;193:385–404.
[8] Ryu Je-Seon, Kim Min-Soo, Cha Kyung-Joon, Lee Tae Hee, Choi Dong-Hoon. Kriging interpolation methods in geostatistics and DACE model. KSME Int J 2002;16(5):619–32.
[9] Jeong Shinkyu, Mitsuhiro Murayama, Kazuomi Yamamoto. Efficient optimization design method using Kriging model. J Aircraft 2005;42(2):413–20.
[10] Hanefi Bayraktar, Turalioglu Sezer F. A Kriging-based approach for locating a sampling site—in the assessment of air quality. Stochastic Environ Res Risk Assess 2005;19(4):301–5.
[11] Den Hertog D, Kleijnen JPC, Siem AYD. The correct Kriging variance estimated by bootstrapping. J Operational Res Soc 2006;57(4):400–9.
[12] Emery Xavier. Simple and ordinary multigaussian Kriging for estimating recoverable reserves. Math Geol 2005;37(3):295–319.
[13] Martin JD, Simpson TW. On using Kriging models as probabilistic models in design. SAE Trans J Mater Manuf 2004;5:129–39.
[14] Shimoyama Koji, Kawai Soshi, Alonso Juan J. Dynamic adaptive sampling based on Kriging surrogate models for efficient uncertainty quantification, Proceeding of 54th AIAA/ASME/ASCE/AHS/ASC Structures, Structural Dynamics, and Materials Conference, Boston, Massachusetts, USA; April 8–11, 2013.
[15] Goyal VK, Kapania RK. Dynamic stability of uncertain laminated beams subjected to subtangential loads. Int J Solids Struct 2008;45(10):2799–817.
[16] Shaker Afeefa, Abdelrahman Wael G, Tawfik Mohammad, Sadek Edward. Stochastic finite element analysis of the free vibration of laminated composite plates. Comput Mech 2008;41:495–501.
[17] Ghavanloo E, Fazelzadeh SA. Free vibration analysis of orthotropic doubly curved shallow shells based on the gradient elasticity. Compos Part B: Eng 2013;45(1):1448–57.
[18] Fazzolari FA. A refined dynamic stiffness element for free vibration analysis of cross-ply laminated composite cylindrical and spherical shallow shells. Compos Part B: Eng 2014;62:143–58.
[19] Tornabene F, Fantuzzi N, Bacciocchi M. Free vibrations of free-form doubly curved shells made of functionally graded materials using higher-order equivalent single layer theories. Compos Part B: Eng 2014;67:490–509.
[20] Mantari JL, Oktem AS, Guedes Soares C. Bending and free vibration analysis of isotropic and multilayered plates and shells by using a new accurate higher-order shear deformation theory. Compos Part B: Eng 2012;43(8):3348–60.
[21] Fang Chin, Springer George S. Design of composite laminates by a Monte Carlo method. Compos Mater 1993;27(7):721–53.
[22] Giunta G, Biscani F, Belouettar S, Carrera E. Hierarchical modelling of doubly curved laminated composite shells under distributed and localised loadings. Compos Part B: Eng 2011;42(4):682–91.
[23] Bruno D, Lato S, Zinno R. Nonlinear analysis of doubly curved composite shells of bimodular material. Compos Eng 1993;3(5):419–35.
[24] Cho M, Kim JS. A post-process method for laminated shells with a doubly curved nine-noded finite element. Compos Part B: Eng 2000;31(1):65–74.
[25] Talha Md, Singh BN. Stochastic perturbation-based finite element for buckling statistics of FGM plates with uncertain material properties in thermal environments. Compos Struct 2014;108:823–33.
[26] Hu HT, Peng HW. Maximization of fundamental frequency of axially compressed laminated curved panels with cutouts. Compos Part B: Eng 2013;47:8–25.
[27] Scarth Carl, Cooper JE, Weaver PM, Silva Gustavo HC. Uncertainty quantification of aeroelastic stability of composite plate wings using lamination parameters. Compos Struct 2014;116:84–93.
[28] Alkhateb H, Al-Ostaz A, Alzebdeh KI. Developing a stochastic model to predict the strength and crack path of random composites. Compos Part B: Eng 2009;40(1):7–16.
[29] Chiachio M, Chiachio J, Rus G. Reliability in composites – a selective review and survey of current development. Compos Part B: Eng 2012;43(3):902–13.
[30] Mahadevan S, Liu X, Xiao Q. A probabilistic progressive failure model for composite laminates. J Reinf Plastics Compos 1997;16(11):1020–38.
[31] Tornabene F, Fantuzzi N, Viola E, Reddy JN. Winkler–Pasternak foundation effect on the static and dynamic analyses of laminated doubly-curved and degenerate shells and panels. Compos Part B: Eng 2014;57:269–96.
[32] Zaman K, McDonald M, Mahadevan S. A probabilistic approach for representation of interval uncertainty. Reliab Eng Syst Saf 2011;96(1):117–30.
[33] Oktem AS, Guedes Soares C. Boundary discontinuous Fourier solution for plates and doubly curved panels using a higher order theory. Compos Part B: Eng 2011;42(4):842–50.
[34] Sriramula S, Chryssanthopoulos MK. Quantification of uncertainty modelling in stochastic analysis of FRP composites. Compos Part A: Appl Sci Manuf 2009;40(11):1673–84.
[35] Shaw A, Sriramula S, Gosling PD, Chryssanthopoulos MK. A critical reliability evaluation of fibre reinforced composite materials based on probabilistic micro and macro-mechanical analysis. Compos Part B: Eng 2010;41(6):446–53.
[36] Carrere N, Rollet Y, Leroy FH, Maire JF. Efficient structural computations with parameters uncertainty for composite applications. Compos Sci Technol 2009;69:1328–33.
[37] Chowdhury R, Adhikari S. Fuzzy parametric uncertainty analysis of linear dynamical systems: a surrogate modeling approach. Mech Syst Signal Process 2012;32:5–17.
[38] Sarangapani G, Ganguli R. Effect of ply level material uncertainty on composite elastic couplings in laminated plates. Int J Comput Methods Eng Sci Mech 2013;14(3):244–61.
[39] Chakravorty D, Bandyopadhyay JN, Sinha PK. Free vibration analysis of point supported laminated composite doubly curved shells – a finite element approach. Comput Struct 1995;54(2):191–8.
[40] Bathe KJ. Finite element procedures in engineering analysis. New Delhi: PHI; 1990.
[41] Meirovitch L. Dynamics and control of structures. New York: John Wiley & Sons; 1992.
[42] Dey S, Karmakar A. Free vibration analyses of multiple delaminated angle-ply composite conical shells – a finite element approach. Compos Struct 2012;94(7):2188–96.
[43] Rayleigh JW. Theory of Sound, re-issue, 1945, second ed. Dover Publications, New York; 1877.
[44] Sacks J, Schiller SB, Welch WJ. Designs for computer experiments. Technometrics 1989;31(1):41–7.
[45] McKay MD, Beckman RJ, Conover WJ. A comparison of three methods for selecting values of input variables in the analysis of output from a computer code. Technometrics 2000;42(1):55–61.
[46] Qatu MS, Leissa AW. Natural frequencies for cantilevered doubly curved laminated composite shallow shells. Compos Struct 1991;17:227–55.
[47] Qatu MS, Leissa AW. Vibration studies for laminated composite twisted cantilever plates. Int J Mech Sci 1991;33(11):927–40.
[48] Leissa AW, Narita Y. Vibrations of corner point supported shallow shells of rectangular planform. Earthquake Eng Struct Dynam 1984;12:651–61.